Tensile properties and microstructural features of 304L austenitic stainless steel produced by wire-and-arc additive manufacturing

Laghi, V., Palermo, M., Tonelli, L. et al.

Tensile properties and microstructural features of 304L austenitic stainless steel produced by wire-and-arc additive manufacturing.

In: International Journal of Advanced Manufacturing Technology 106, 3693–3705 (2020)

Tensile properties and microstructural features of 304L austenitic stainless steel produced by Wire-and-Arc Additive Manufacturing

Vittoria Laghi[1]*, Michele Palermo Ph.D[1], Lavinia Tonelli[2], Giada Gasparini Ph.D[1], Lorella Ceschini Ph.D[1], Tomaso Trombetti Ph.D[1]

*corresponding author: vittoria.laghi2@unibo.it
ORCiD ID: https://orcid.org/0000-0001-8395-2194

[1]Department of Civil, Chemical, Environmental and Materials Engineering (DICAM) - University of Bologna, Viale del Risorgimento, 2 – 40136 Bologna, Italy

[2]Department of Industrial Engineering (DIN) - University of Bologna, Bologna (Italy)

Tensile properties and microstructural features of 304L austenitic stainless steel produced by Wire-and-Arc Additive Manufacturing

Abstract

Additive manufacturing (AM) has gained great importance in the recent development to produce metallic structural elements for civil engineering applications. However, research effort has been focused mainly on powder-based processes, while there is still limited knowledge concerning the structural response of Wire-and-Arc Additive Manufactured (WAAM) metallic elements, and very few experimental data concerning their mechanical properties. This paper presents the first results of a wide experimental campaign aimed at assessing the mechanical properties of WAAM plates produced using a commercial ER308LSi stainless steel welding wire. The aim is to evaluate the effect of the orientation in the tensile behavior of planar elements considering specimens extracted in three different directions with respect to the deposition layer: (i) transversal direction (T), (ii) longitudinal direction (L) and (iii) diagonal direction (D). Compositional, microstructural and fractographic analyses were carried out to relate the specific microstructural features induced by WAAM to the mechanical properties. The results show that the chemical composition of the plates meets the requirements of UNS-S-30403 for an AISI 304L austenitic stainless steel. The as-built samples were substantially defect-free and characterized by a very fine microstructure of γ and δ phases. The fineness of the microstructure and the negligible defect content led to values of tensile strength and elongation to failure in line with the traditionally manufactured stainless steel elements. Anisotropy in the tensile properties between T, L and D specimens was observed and the highest elastic and plastic properties were measured in D specimens. This result is related to the crystallographic and mechanical fibering induced by the additive process, that led also, in case of D samples, to the highest density of cell boundaries, obstacles to the dislocation slip, located at 45° with respect to the loading direction, where plastic deformation preferentially occurs.

Key words

Additive Manufacturing; Wire-and-arc; Austenitic stainless steel; Mechanical behavior; Microstructural analysis.

1. Introduction

Within the category of AM processes, Wire-and-Arc Additive Manufacturing (WAAM) is the most suitable for realizing large-scale metal parts for Structural Engineering purposes [1]. According to ASTM F 2792-10 [2], WAAM lies within the category of Direct Energy Deposition (DED) processes, and it is defined as the combination of an electric arc as thermal source to melt the wire feedstock and deposit a part pre-form, layer by layer [3]. According to the different heat source adopted, WAAM technologies can be distinguished into: Gas Tungsten Arc welding (GTAW), Gas Metal Arc Welding (GMAW) and Plasma Arc Welding (PAW). WAAM processes are based on the layer-by-layer deposition of molten metallic material, while the motion mechanism is provided by an articulated industrial robot, which is computer-guided in order to follow the desired path to build the full-dense part. The main advantages of such innovative manufacturing technology lie upon the wide freedom in realizing any sort of designed geometry, with more controlled material usage both in terms of waste and weight reduction. Among the different metal 3D printing strategies, WAAM technique allows higher deposition rates, resulting to be more prone to realize large real-scale structural components and guarantee lower costs compared to other AM techniques for metals [4–6].

Although much research effort has been devoted to assess Powder Based Fusion (PBF) and powder-based DED materials [7–9], nowadays there is limited amount of research work concerning the influence of WAAM process parameters on the material properties [10,11]. Among WAAM processed stainless steels, the available literature reports limited data about maraging steel [12], 2Cr13 martensitic stainless steel [13], 316L [14–16] and 304L [17–19] austenitic stainless steels, as well as 2209 duplex stainless steel [20]. The presented results are focused on the assessment of the influence of the orientations with respect to the deposition layer on the tensile strengths (yielding and ultimate tensile strengths) of WAAM metallic specimens, hence confirming the interest in studying the anisotropy of the printed outcomes. In the work done by Gordon and co-authors [14], also Young's modulus values are reported, indicating values around 130 to 140 GPa, significantly lower than the one registered by the conventional wrought material (about 190 GPa). Wu and co-workers [15] found a first correlation between the tensile strength and the specimens orientation, in terms of orientation of grain growth. Thus, it is crucial to perform a proper investigation of WAAM stainless steel material properties, with focus to Young's modulus values with respect to the specimens orientation, coupled with a specific microstructural characterization.

The limited literature work focused on this innovative process does not emphasize the potential anisotropy induced by the process in the tensile properties of the printed outcomes. Furthermore, very few studies emphasize the effect of the specific microstructural features

influencing the mechanical behavior [11,12]. Thus, recent investigations by some of the authors on WAAM-produced stainless steel structural elements studied the anisotropic behavior depending on the printing direction [21], suggesting some peculiar dependency of the inherent material properties on the orientation of the specimen.

In light of the above-mentioned issues, the focus of the present work is to investigate the influence of elements orientation on the tensile properties of WAAM plates produced using a commercial austenitic ER308LSi wire, through both mechanical and microstructural characterization.

2. Experimental methods

A wide experimental campaign has been carried out to characterize a series of planar specimens cut from plates realized with WAAM process and ER308LSi wire. A total of ten plates with nominal dimensions of 380 x 380 x 4 mm^3 have been realized at MX3D facilities [22].

In order to evaluate possible anisotropy induced by the process, the tested specimens have been cut from the plates following three main orientations with respect to the deposition layer: (i) longitudinal (L), i.e. parallel to the deposition layer; transversal (T), i.e. perpendicular to the deposition layer; (iii) diagonal (D), i.e. at 45° with respect to the deposition layer. Tensile and metallographic samples have been extracted following the scheme provided in Figure 1.

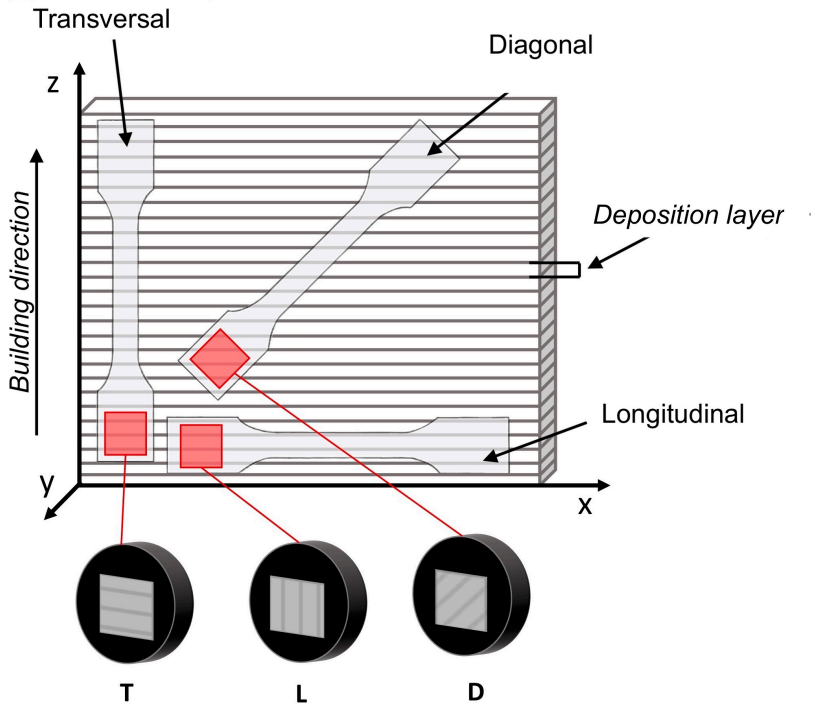

Fig 1 *Orientation of the tensile specimens cut from WAAM plates with respect to the deposition layer and scheme of extraction of the metallographic samples for the microstructural characterization*

A series of experimental tests have been performed, in order to characterize the mechanical properties of WAAM stainless steel (described in Section 2.2), as well as the chemical composition, microstructure and fractography (described in Section 2.3).

2.1. Material and process

A commercially available standard stainless steel welding wire grade ER308LSi (1 mm diameter) supplied by *Oerlikon* [23] was used to manufacture the WAAM plates provided by MX3D [22] according to the process parameters reported in Table 1.

Process parameters	**Details**	**Value**
Deposition power	Current Arc voltage	100 - 140 A 18 - 21 V
Speed	Welding speed Wire feed rate Deposit rate	15 - 30 mm/s 4 - 8 m/min 0.5 - 2 kg/h
Distance and angle	Layer height Electrode to layer angle	0.5 - 2 mm 90°
Wire	Wire grade Wire diameter	ER308LSi 1 mm
Shield gas	Shield gas type Shield gas flow rate	98% Ar, 2%CO_2 10-20 L/min

Table 1: Process parameters for WAAM deposition (Courtesy of MX3D [22]*).*

In order to increase the overall printing velocity, active cooling system has been adopted, consisting of blowing compressed air on the printed layer before depositing the successive one, thus reducing the waiting time between two deposition layers.

2.2. Mechanical characterization

Tensile and hardness tests were conducted on a total number of 9 specimens (3 per direction) to assess the mechanical properties of WAAM planar elements. The specimens, extracted along the three main directions as shown in Figure 1, were shaped according to ISO 6892-1 [24] (Figure 2).

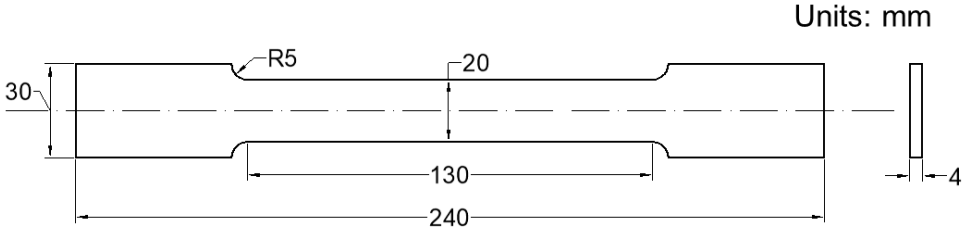

Fig 2 *Geometry and dimensions (mm) of the flat tensile specimens according to ISO 6892-1* [24]

Given the rough nature of the printed plates, proper of the WAAM process [21,25], the surface of the tensile specimens has been polished by means of mechanical milling, reducing the final thickness to an average value of 2.5 to 3 mm, starting from the nominal 4-mm thickness of the plates. In fact, tensile tests with the as-printed topography would be affected by the cross-sectional variation, thus altering the determination of the resisting cross-section. As such, previous studies have been conducted on as-printed specimens, and evaluated considering an effective homogeneous cross-sectional area taken from volume equivalency [21,25]. Images of the specimens before and after milling are shown in Figure 3 (a-b). Surface topography images obtained by 3D-Digital Microscopy (Hirox KH-7700) before and after polishing are compared in Figure 3 (c-d). As can be noted from 3D reconstructions, the as-printed surface is characterized by a consistent waviness, due to the layer-by-layer deposition strategy. After the milling process, the waviness is removed and the roughness significantly reduced, thus allowing to consider the surface substantially flat. The surface roughness of the polished specimen has been measured with stylus profilometry (Hommelwerke T200, 5 µm tip radius), and it resulted equal to Ra=0.53±0.06 µm and Rz=5±0.12 µm.

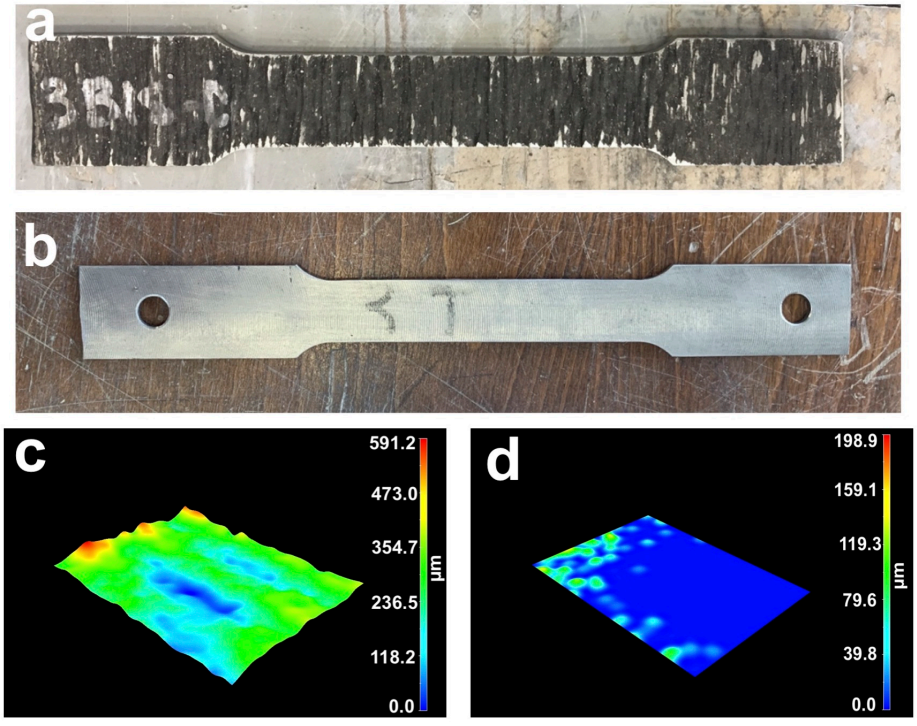

Fig 3 *Tensile specimen cut from WAAM plates: (a) as-printed and (b) after surface milling; surface topography images obtained with 3D-Digital Microscopy of the specimen (c) as-printed and (b) after surface milling*

The tensile tests have been performed according to ISO 6892-1 [24] on a Universal testing machine of 500 kN load capacity. The specimens have been tested in displacement-control having a velocity of 2 MPa/s. Two types of monitoring systems have been adopted: a linear deformometer of nominal dimension of 50 mm, to detect the linear deformation of the specimens up to yielding, and an optical-based system referred to as Digital Image Correlation (DIC), to acquire the full strain field during the whole test until failure.

Three specimens for each extraction direction (according to the scheme reported in Fig. 1) were tested. Before testing, the dimensions of the specimens have been measured by means of digital caliper in order to obtain the true values of cross-sectional area, averaged on a total number of 10 measures over the entire length. The average values of the main geometrical dimensions (mean value and standard deviation of thickness t and average cross-sectional area A_m) are reported in Table 2.

The density of WAAM samples was determined by means of volume-based measures taken with a hydraulic scale according to the Archimedes' principle.

Specimen ID	**t [mm]**	**A_m [mm^2]**
1-L	3.10 ± 0.19	101.22
2-L	3.01 ± 0.18	89.49
3-L	2.48 ± 0.20	78.58
1-D	2.86 ± 0.09	92.98
2-D	3.35 ± 0.27	106.30
3-D	2.87 ± 0.17	87.52
1-T	2.58 ± 0.15	81.91
2-T	2.58 ± 0.08	84.00
3-T	2.57 ± 0.31	82.12

Table 2: Summary of tensile specimens dimensions.

Elastic Modulus (E), 0.2% proof stress ($Rp_{0.2}$), ultimate tensile strength (UTS) and elongation to failure ($A_{\%}$) were evaluated from the engineering stress-strain curves.
Sclerometric measurements were carried out by HV1 Vickers hardness tests (1 kg load, 15 s dwell time).

2.3. Chemical, microstructural and fractographic characterization

The chemical analysis of WAAM plates realized with commercial ER308LSi wire has been checked by Glow Discharge Optical Emission Spectroscopy (GDOES: GDA-650, Spectruma Analytik GmbH, Hof, Germany), with a sputtered burnt spot of 4 mm diameter, in order to determine the composition of the newly produced material compared with the one of the feedstock wire.

To relate the mechanical behavior with specific microstructural features induced by the process, microstructural analyses were carried out by means of 3D-Digital Microscopy (Hirox KH-7700), Reflected Light Optical Microscopy (RLOM) and Scanning Electron Microscopy (SEM) equipped with energy dispersive X-ray spectroscopy (EDS). Samples for microstructural characterization have been cut from grip regions of longitudinal, transversal and diagonal tensile specimens, according to the scheme shown in Fig.1. The samples were mounted in a phenolic resin, grounded with silicon carbide papers up to 2000 grits and finally polished according to ASTM E3 standard [26] with 1 μm polycrystalline diamond suspension to obtain a mirror finish. In order to highlight any specific microstructural features induced by WAAM, chemical etching with 20s immersion in the Vilella's reagent (1 g picric acid, 5 mL hydrochloric acid and 100 mL ethanol) was performed [27]. Quantitative image analysis was carried out by ImageJ software [28] on low magnification micrographs (50x, 3D-Digital Microscope) over at least 15 images to evaluate the average thickness of the deposition layer.

After the tensile tests, specimens fracture surfaces were analyzed both at low magnification by 3D-Digital Microscopy and at higher magnification with SEM-EDS to investigate the specific failure mechanisms.

3. Results and discussion

3.1 Compositional analysis

GD-OES compositional analysis was performed on the printed steel plates and results are reported in Table 3, where the composition of the feedstock wire is reported as well. Since type ER 308LSi is the common filler wire used in the conventional welding processes of austenitic stainless steel 304L, results of WAAM plates were also compared to the 304L (UNS-S-30403), whose chemical composition is still reported for an easy reference in Table 3. From the comparison, it can be inferred that the composition of WAAM samples meets the requirements of UNS-S-30403 for an AISI 304L chromium-nickel austenitic stainless steel. So, hereafter all results on the WAAM samples are compared to the properties of 304L stainless steel.

	C	***Cr***	***Ni***	***Mn***	***Si***	***Co***	***V***	***Mo***	***Cu***	***P***	***S***	***Fe***
Wire	0.02	20	10	1.8	0.85	-	-	0.2	-	<0.025	<0.020	Bal.
WAAM Samples	0.009	19.495	9.583	1.73	0.634	0.471	0.111	0.015	0.015	0.0222	0.0113	Bal.
AISI 304L	<0.03	18.0-20.0	8.0-12.0	<2.0	<1.0	-	-	-	-	<0.045	<0.03	Bal.

Table 3: Results of the GD-OES composition analysis (wt.%) performed on the WAAM samples compared to the nominal chemical composition of the wire (given by the supplier) and 304L (UNS-S-30403) austenitic stainless steels according to ASTM A276 [29] *respectively.*

3.2 Microstructural characterization

Figure 4 shows the typical microstructures of WAAM-processed alloys, obtained by 3D digital microscopy at relatively low magnification on metallographic samples extracted from the grip regions of T (a), L (b) and D (c) tensile specimens, according to the scheme in Fig.1.

A common issue for welding-related processes (like WAAM) is the controlled porosity. In this regard, no macroscopic defect (e.g. cracks, porosity, or lack of fusion) was evidenced by metallographic analyses in the majority of the as-printed samples between any two adjacent layers. Thus, the process resulted in mainly defect-free plates with a dense structure. Further evidences of this aspect are found in the density measurements of the printed plates, on average equal to 7930 ± 240 kg/m^3.

The low magnification optical images in Fig.4 clearly show the typical hierarchical microstructure of additively manufactured parts [8], induced by the layer-by-layer process and the rapid

solidification of the molten material. In the micrographs, deposition layers are highlighted by red lines, columnar grains by yellow lines and the fine cellular sub-structure by green lines.

The height of the deposition layers is found regular and equal to about 1.04 ± 0.34 mm (according to the printing parameter used as input, see Table 1), as it can be appreciated from the red lines in Fig. 4. Deposition layers are perpendicular, parallel and 45° oriented with respect to loading direction in specimens T, L and D, respectively.

From the micrographs in Fig.4 it can also be appreciated that the macro morphology throughout the X-Z plane of the WAAM plate is dominated by columnar grains, with a preferential texture along the building (Z) direction, perpendicular to the bottom substrate up to the top section. The extension of the grains across several deposition layers, has already been encountered in other studies concerning WAAM processes [14,30]. Indeed, such morphology is strictly dependent on the specific nature of WAAM technology, that essentially consists of an additive multi-pass welding process, in which during each deposition the upper part of the former layer is re-melted and leaves the columnar grains in the former layer partially melted. When solidification occurs, the grain growth direction is perpendicular to the solid/liquid interface so to follow the maximum temperature gradient [31]. As a result, the partially remelted columnar grains in the former layer further grow and develop through the entire buildup component. The final microstructure of the deposited stainless steel is therefore dependent on the maximum temperature, time at temperature and cooling rate during the multiple thermal cycles experienced by each layer of deposited material. In addition, these columnar grains crossing over layers follow an epitaxial growth: as evidenced by the microstructure in Fig.5, and especially by the polarized micrograph reported in Fig.5a, the liquid metal solidifies by replicating the growing direction of the previous layer. As it can be seen on micrographs in Fig.4, the width of these columnar grains can extend up to over 500 μm. High magnification analyses (Fig.5 and Fig.6) revealed a fine cellular sub-structure within the larger columnar grains, whose size is of the order of few microns, as confirmed by Fig.6b, and consists of primary γ-austenite dendrites and δ-ferrite at the cell boundaries. It is known that solidification in austenitic stainless steel welds is related to the composition of the alloy. For the case studied, according to the GD-OES results reported in Table 3, since Cr_{eq}=20.461% and Ni_{eq}=10.718%, according to the Schaeffler diagram [32], the welds should solidify with the austenite being the primary or leading phase and the δ-ferrite located in the interdendritic spaces.

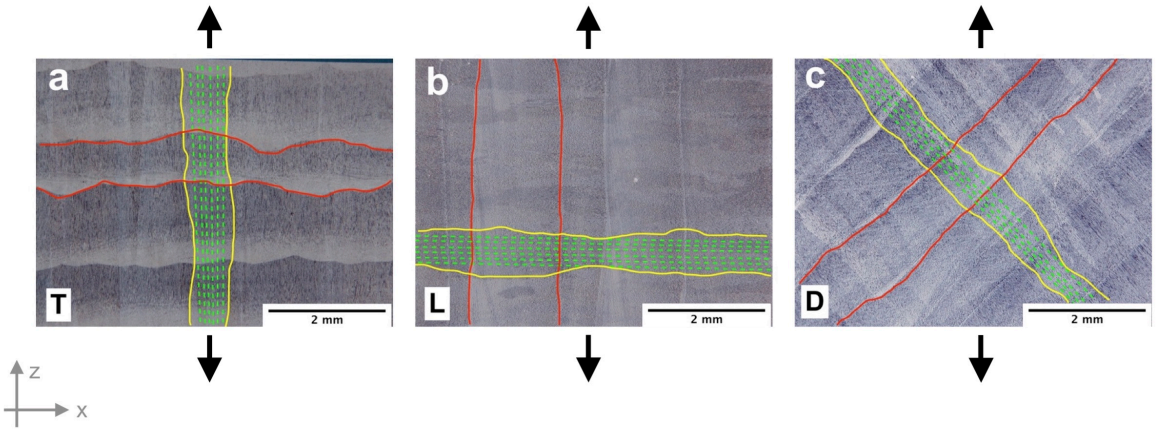

Fig 4 *Representative low magnification 3D Digital micrographs of: a) transverse, b) longitudinal and c) diagonal tensile samples (Fig.1), where deposition layer, epitaxial grain growth and cellular sub-structures directions are highlighted by red, yellow and green lines, respectively; black arrows indicates the loading direction.*

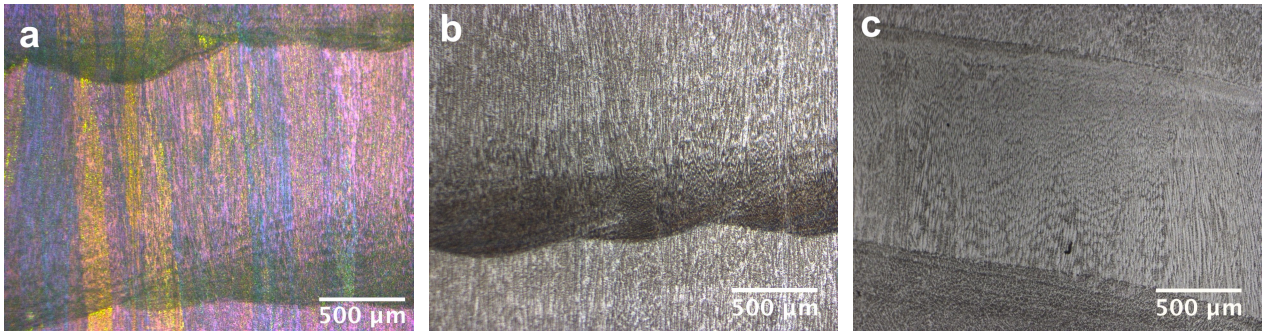

Fig 5 *Optical micrographs of the interfacial layer between weld lines: a) polarized filter, b) and c) bright field.*

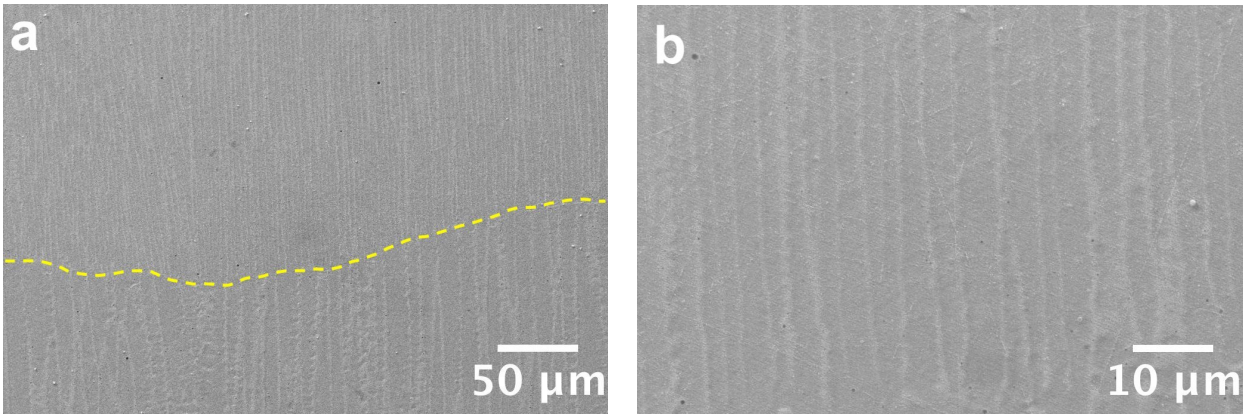

Fig 6 *SEM micrographs of: a) the interfacial layer between weld line, where yellow dotted line represents the layer border; b) high magnification of the lower region (i.e. next to the border) of a layer*

3.3 Tensile and hardness data

Figure 7 shows the whole engineering stress-strain curves and a zoom of them corresponding to a strain limit of 1%, for specimens T (Figure 7a,b), L (Figure 7c,d) and D (Figure 7e,f).

The curves show in general a quite-uniform stress-strain behavior for the three specimens orientations considered, except for the strain values registered for specimens T (Figure 7a), for which a considerable variation in the population response is encountered. This is due to inherent defects in the specimen with the lowest elongation to failure (specimen 3-T), as presented in more details in the analysis of fracture surfaces in Section 3.4.

Considering the first part of the curves, up to the first yielding point (Figures 7b,d,f), it is clearly appreciable a stiffer elastic behavior of the specimens D, showing almost double Young's modulus value on average with respect to the other two directions. This is also evident in the strain values of elastic limit: for specimens D, strain values are around 0.2%, lower than those for the other two directions, which are around 0.3%. On average, along all the three orientations, a ductile behavior is evidenced, with values of elongation to failure in the range of 20 to 25%.

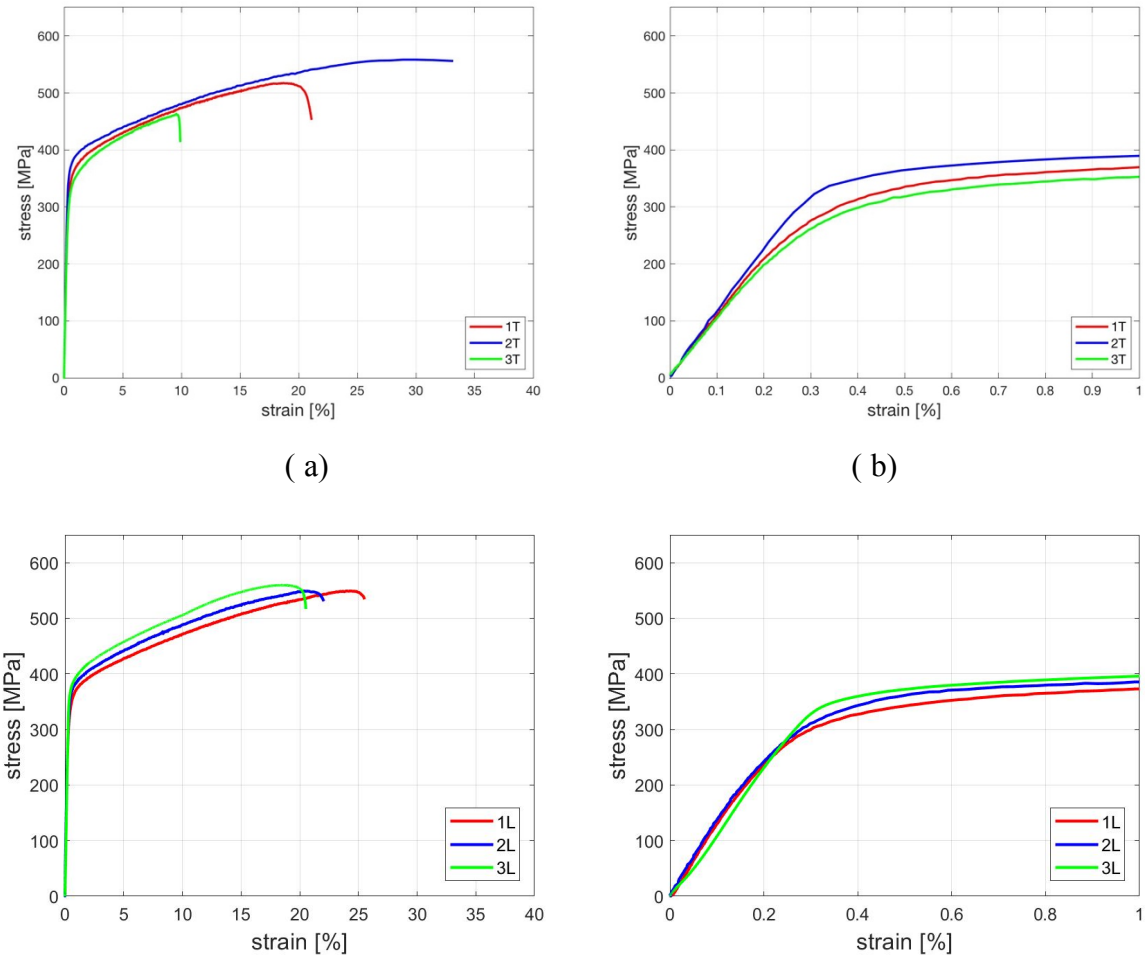

(c) (d)

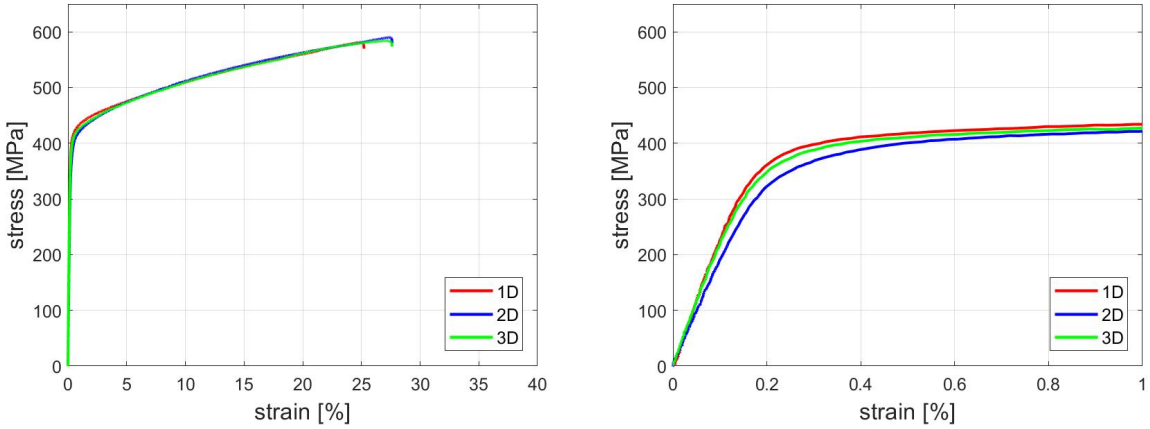

(e) (f)

Fig 7 *Stress-strain curves for tensile tests: (a) specimens T and (b) a zoom of them; (c) specimens L and (d) a zoom of them; (e) specimens D and (f) a zoom of them*

Table 5 reports the values of the key material parameters computed from tensile tests according to EN ISO 6892-1 [24] standards, in terms of Young's modulus (*E*), 0.2% proof stress ($R_{p0.2}$), ultimate tensile strength (*UTS*), elongation to failure ($A_{\%}$) and yield to tensile strength ratio ($R_{p0.2}$/ *UTS*).

Specimen ID	**E [GPa]**	**$R_{p0.2}$ [MPa]**	**UTS [MPa]**	**$A_{\%}$ [%]**	**$R_{p0.2}$/ UTS**
1-T	103.27	367.22	517.42	21.11	0.71
2-T	109.14	362.14	558.41	33.18	0.65
3-T	102.12	325.06	463.58	9.93	0.70
μ	**104.84 ± 3.15**	**351.47 ± 17.57**	**513.14 ± 41.05**	**21.41 ± 9.42**	**0.69 ± 0.03**
1-L	131.82	342.91	549.10	25.54	0.62
2-L	126.62	353.50	549.07	22.06	0.62
3-L	127.58	370.79	559.62	20.52	0.66
μ	**128.68 ± 2.57**	**355.73 ± 10.67**	**552.60 ± 5.53**	**22.71 ± 2.04**	**0.64 ± 0.01**
1-D	261.01	418.37	581.21	25.22	0.72

2-D	185.86	382.30	589.93	27.62	0.65
3-D	236.44	408.73	583.96	27.61	0.70
μ	**227.77 ± 31.89**	**403.13 ± 16.13**	**585.03 ± 5.85**	**26.82 ± 1.07**	**0.69 ± 0.03**

Table 5: Summary of tensile tests results.

The histograms of Figure 8 provide a graphical comparison of the mechanical properties for the three orientations of the specimens tested (T, L and D). The trends for the main mechanical properties are similar with respect to the orientation of the specimens, clearly indicating an anisotropic behavior of the WAAM stainless steel material. Indeed, as also evidenced from the relative ratios in Table 6, the mechanical properties for specimens T are slightly lower than those for specimens L, which in comparison are significantly lower with respect to those for specimens D. The highest anisotropy is registered for Young's modulus, whose results are more than double for specimens D with respect to those along T, and almost double with respect to those along L. Specimens L and T exhibited similar mechanical properties, both in terms of 0.2% proof stress (about 350 MPa), ultimate tensile strength (in the range 510-550 MPa) and elongation to failure (20-25%). On the other hand, specimens D showed slightly higher tensile properties, with a 0.2% proof strength of about 400 MPa, an ultimate tensile strength over 580 MPa and 27% of elongation. Noteworthy is the influence of the specimens orientation in the values of Young's modulus, much higher for specimens D (average value of 230 GPa) with respect to specimens L (average value of 130 GPa) and T (average value of 105 GPa). Similar results in terms of reduction of Young's modulus and influence in the specimens orientation is found in [33], although the experiments were conducted on 316L stainless steel realized with Selective Laser Melting process.

Overall, given the low values of deviations of the results obtained for the main mechanical properties for each orientation, the results provide a good first evaluation of the main mechanical properties of WAAM-produced 304L stainless steel specimens. Similar trends and anisotropic behavior is also presented in the work done by Gardner and co-workers in [19].

Relative ratio	**E [-]**	**$R_{p0.2}$ [-]**	**UTS [MPa]**	**$A_{\%}$ [%]**
L / T	1.23	1.01	1.08	1.06

D / T	2.17	1.15	1.14	1.25
D / L	1.77	1.13	1.06	1.18

Table 6: Relative ratios of the main mechanical properties with respect to the orientation of specimens.

The observed anisotropy in the behavior of WAAM specimens might be related to the different grain orientations, with respect to the loading direction, shown in Fig.4.

It is well known that under uniaxial tensile loading, plastic deformation of metals preferentially occurs along slip planes oriented at 45° with respect to the loading direction, where shear stress reaches its maximum value [34]. Hindering dislocation slip, which is responsible for plastic deformation, by strengthening mechanisms, allows increasing tensile strength. Several studies demonstrate that grain refinement is the one of the most effective strengthening mechanisms in SLM parts, enhancing both strength and elongation, due to the high solidification rate induced by the process [35]. In the hierarchical microstructure typical of additively manufactured parts, the first obstacle to dislocation slip is the cellular sub-structure (few micrometers in the present study). The observed anisotropy in the tensile properties of WAAM 304 L stainless steel samples should be likely related to the different orientations of this fine cellular sub-structure among T, L and D specimens, schematically shown in Fig.4. The superior tensile properties in terms of yield and ultimate tensile strength observed in D samples can be related to the highest density of cells boundaries along the main slip direction oriented at 45° to the tensile loading. It is worth noting that specimens D also exhibited the highest elastic modulus, clearly related to crystallographic and mechanical fibering, that are widely reported as the main reasons for the elastic anisotropy of metals [34,36].

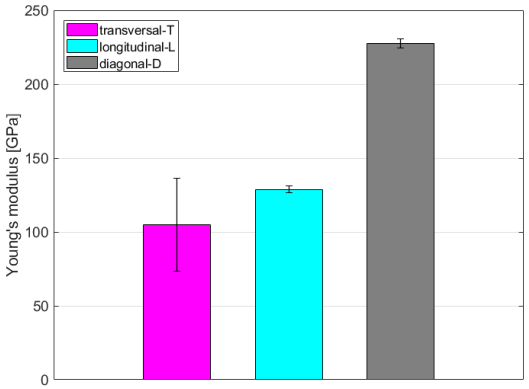

(a)

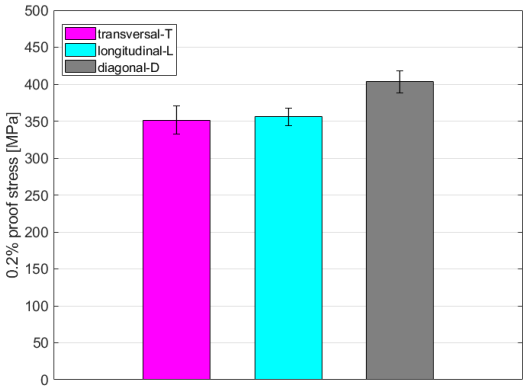

(b)

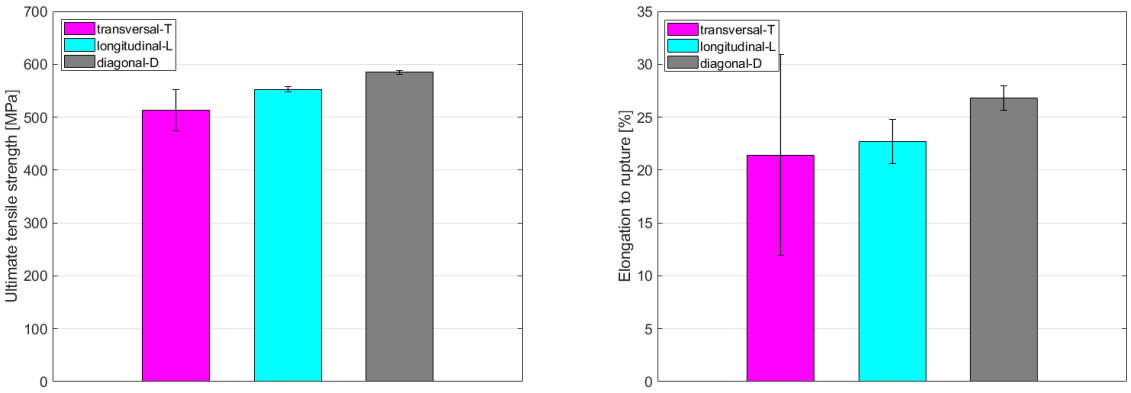

(c) (d)

Fig 8 *Results of the tensile tests on longitudinal, diagonal and transversal specimens cut from WAAM plates according to the scheme in Fig.1: (a) Young's modulus; (b) 0.2% proof stress; (c) ultimate tensile strength; (d) elongation to failure*

A summary of results found in literature for the additively manufactured AISI 304L is presented in Table 6, including reference values to international standard building codes [37–39] for the conventional wrought material. It is worth noting that only L and T specimens were considered in the literature, while no data are reported on specimens D, with a diagonal orientation with respect to the deposition layer.

By comparing the results of the present study with the outcomes of previous studies on the 304L produced by WAAM, it can be noticed that, in accordance with the present study, no evidence of a strong anisotropy between L and T direction was found. Only one paper [14] reported Young's modulus data, showing a comparable value both for the L and T direction of about 135 GPa, consistent with the results of the present study. The same considerations can be applied also for the other DED processes reported in Table 6, even if it is worth mentioning that in one case ([40], also reported in[13]) a significant anisotropy was found between L and T orientation, being the T one the most penalized, as for the present work. Finally, it is evident that for Powder-Based Fusion (PBF) processes, such as Selective Laser Melting (SLM), the values of 0.2% proof stress and ultimate tensile strengths are quite higher (30 to 40% higher) than the ones registered for Directed Energy Deposition (DED) processes, like WAAM. A possible explanation can be related to the finer microstructure resulting from PBF processes, with respect to the DED ones [31], since it is well known that grain refinement is the only strengthening mechanism that simultaneously increases both strength and ductility. By comparing the results of the present study with the international standard building codes

[37–39], it can be noted that 0.2% proof stress of the WAAM processed 304L steel is higher than the standard requested for the wrought material while the ultimate tensile strength is comparable. The strong difference is represented by the value of the Young's modulus, as already discussed, higher for the D specimens while consistently lower than the one required by the standards in the case of L and T specimens.

	Process type	**Specimen orientation**	**E [GPa]**	**$R_{p0.2}$ [MPa]**	**UTS [MPa]**	**$A_{\%}$ [%]**	**Reference**
PRESENT STUDY							
WAAM	GMAW	T	105	351	513	21	/
		L	129	356	553	23	
		D	228	403	585	27	
LITERATURE REVIEW							
WAAM	GMAW	L	139	296	524	/	[14]
		T	132	306	499	/	
	GTAW	L	/	231	622	88	[17]
		T	/	235	678	57	
	GMAW	L	/	356	612	/	[18]
Other DED	LENS	L	/	448	710	59	[13]
		T	/	324	655	70	
	L-DED	L	/	337	609	48	[13,40]
		T	/	314	606	56	
	LMD	L	/	337	609	48	[17,40]
		T	/	314	606	56	
PBF	SLM	L	/	520	710	38	[13]
		T	/	450	580	58	

	SLM	L T	/ /	535 455	693 580	42 58	[17]
Wrought	/	/	200	190 - 230	500 - 540	/	[37]
	/	/	195	195 - 205	520	/	[38]
	/	/	193.1	247.2 – 275.8	551.6 – 620.6	/	[39]

Table 6: Summary of 304L stainless steel tensile properties from literature review [13,14,17,18,40]*, classified according to the type of the process. In the table, LENS stands for Laser Engineered Net Shaped, LMD for Laser Metal Deposition, L-DED Laser-based Direct Energy Deposition, SLM for Selective Laser Melting.*

Hardness measurements (HV_1) have also been performed on polished and etched metallographic specimens, both in correspondence of the weld lines between two subsequent layers and in the core of the layers. The analysis was conducted with the aim of evaluating a possible dissimilarity in the mechanical properties along the deposition layer. Actually, the results showed that hardness of the two investigated areas are comparable and equal to 306±14 HV_1 for the layer core and 307±21 HV_1 for the border.

3.4 Fracture surfaces

Representative images of the tensile fracture surfaces, obtained by multi-focus microscopy at relatively low magnification, are shown in Fig.9, highlighting that no macroscopic defects were present in the majority of the tested samples.

High magnification analyses were also carried out by SEM-EDS to better highlight specific microstructural features of the failure (Figure 10).

Observation of the fracture surfaces by SEM-EDS at very high magnification, reported in Fig.10a, evidenced the presence of very small dimples, about 1 μm in size, in all the tested specimens, independently from specimen orientation, typical of a ductile failure. The fineness of the dimples is clearly related to the corresponding very fine microstructure induced by the WAAM process in the stainless steel. From high magnification analyses, also justifications on the low ultimate strength and elongation to failure value of sample 3-T (lower than 10%) has been found in the presence of a large defect in the fracture surface, shown in Figure 10b.

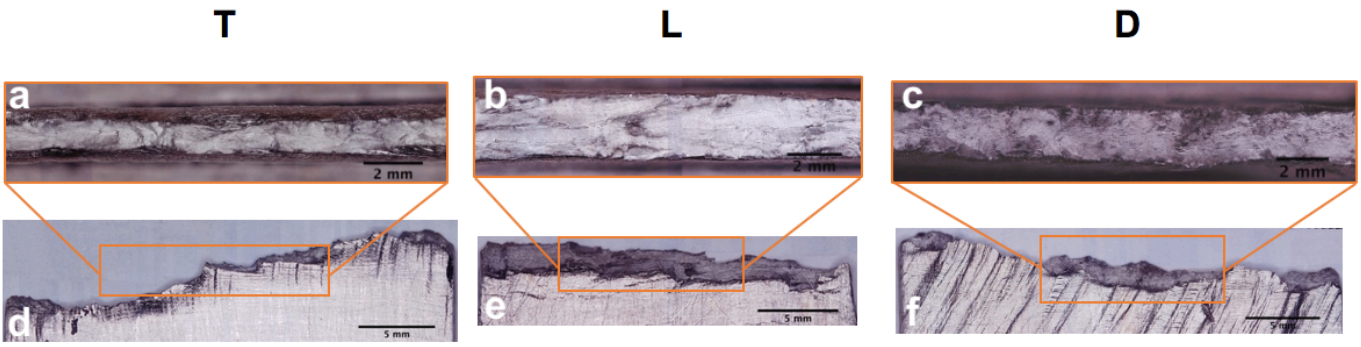

Fig 9 *Low magnification micrographs obtained by 3D multifocus microscopy of the top and lateral view of the fracture region: a) and d) transversal, b) and e) longitudinal, c) and f) diagonal tensile samples*

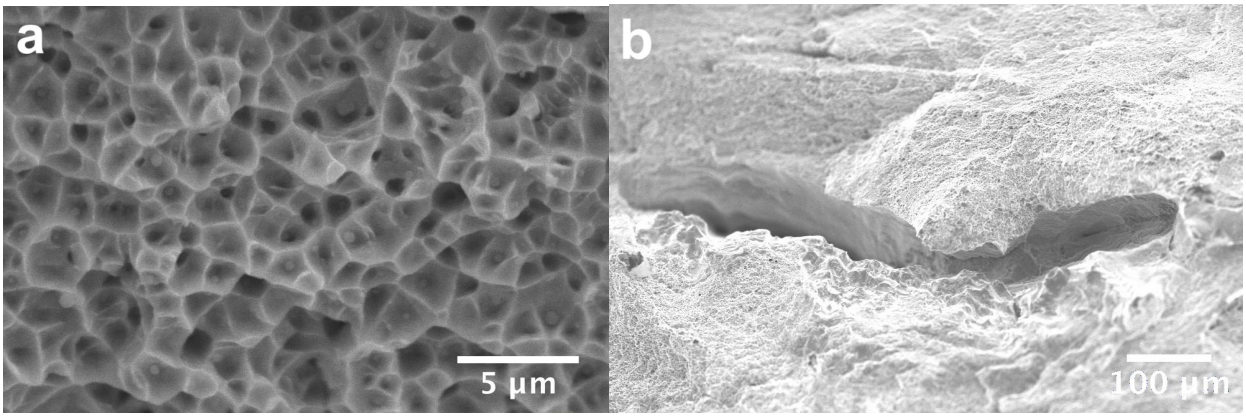

Fig 10 *High magnification SEM micrographs of fracture surfaces: a) representative image reporting fine dimples structure, b) defect found on sample 3T*

Conclusions

In the paper, the results of a first experimental campaign aimed at characterizing the key mechanical properties (Young's modulus, yield and ultimate tensile strength, elongation to failure, hardness), chemical composition and microstructure of Wire-and-Arc Additive Manufacturing (WAAM) austenitic stainless steel are reported. The main goal is to draw some considerations on the potential anisotropic mechanical behavior induced by the microstructure.

The specimens have been cut from plates realized with WAAM process using an ER308LSi wire, with different orientations with respect to the deposition layer: (i) transversal direction (T), (ii) longitudinal direction (L) and (iii) diagonal direction (D).

Chemical analysis showed that the printed material might be considered as a 304L stainless steel. Microstructural characterization at different magnifications revealed a substantially defect-free, full-dense material, confirmed by the density value of about 7900 kg/m^3. The microstructural characterization evidenced a hierarchical microstructure, typical of additively manufactured parts, structured in: deposition layers, epitaxial columnar grains crossing over layers and a fine cellular sub-structure inside the grains.

Tensile tests have been performed on L, T and D specimens, previously treated with surface milling to reduce the surface roughness proper of WAAM process. Anisotropy in the tensile properties was observed, with the highest elastic and plastic properties measured in D specimens. This behavior was related to the crystallographic and mechanical fibering induced by the process that also leads to the highest density of obstacles (cell boundaries) to dislocation slip, that preferentially occurs at 45° with respect to the tensile loading, present in D samples.

SEM analyses of the fracture surfaces confirmed a substantially defect free microstructure, with a typical ductile morphology of very fine equiaxed dimples.

Acknowledgements

The support of Dutch company MX3D held in Amsterdam is gratefully acknowledged for giving the additive-manufactured elements tested.

References

[1] C. Buchanan, L. Gardner, Metal 3D printing in construction: A review of methods, research, applications, opportunities and challenges, Eng. Struct. 180 (2019) 332–348. https://doi.org/10.1016/j.engstruct.2018.11.045.

[2] ASTM, ASTM F 2792-10 Standard Terminology for Additive Manufacturing Technologies, (2010).

[3] T.A. Rodrigues, V. Duarte, R.M. Miranda, T.G. Santos, J.P. Oliveira, Current status and perspectives on wire and arc additive manufacturing (WAAM), Materials (Basel). 12 (2019). https://doi.org/10.3390/ma12071121.

[4] K. V. Wong, A. Hernandez, A Review of Additive Manufacturing, ISRN Mech. Eng. 2012 (2012) 1–10. https://doi.org/10.5402/2012/208760.

[5] S.W. Williams, F. Martina, A.C. Addison, J. Ding, G. Pardal, P. Colegrove, Wire + Arc additive manufacturing, Mater. Sci. Technol. (United Kingdom). 32 (2016) 641–647. https://doi.org/10.1179/1743284715Y.0000000073.

[6] A. Uziel, Looking at large-scale, arc-based Additive Manufacturing, Weld. J. 4 (2016).

[7] C. Buchanan, V.P. Matilainen, A. Salminen, L. Gardner, Structural performance of additive manufactured metallic material and cross-sections, J. Constr. Steel Res. 136 (2017) 35–48. https://doi.org/10.1016/j.jcsr.2017.05.002.

[8] T. DebRoy, H.L. Wei, J.S. Zuback, T. Mukherjee, J.W. Elmer, J.O. Milewski, A.M. Beese, A. Wilson-Heid, A. De, W. Zhang, Additive manufacturing of metallic components – Process, structure and properties, Prog. Mater. Sci. 92 (2018) 112–224. https://doi.org/10.1016/j.pmatsci.2017.10.001.

[9] Y. Zhang, L. Wu, X. Guo, S. Kane, Y. Deng, Y.G. Jung, J.H. Lee, J. Zhang, Additive Manufacturing of Metallic Materials: A Review, J. Mater. Eng. Perform. 27 (2018) 1–13. https://doi.org/10.1007/s11665-017-2747-y.

[10] I.S. Kim, K.J. Son, Y.S. Yang, P.K.D.V. Yaragada, Sensitivity analysis for process parameters in GMA welding processes using a factorial design method, Int. J. Mach. Tools Manuf. 43 (2003) 763–769. https://doi.org/10.1016/S0890-6955(03)00054-3.

[11] M. Dinovitzer, X. Chen, J. Laliberte, X. Huang, H. Frei, Effect of wire and arc additive manufacturing (WAAM) process parameters on bead geometry and microstructure, Addit. Manuf. 26 (2019) 138–146. https://doi.org/10.1016/j.addma.2018.12.013.

[12] X. Xu, S. Ganguly, J. Ding, S. Guo, S. Williams, F. Martina, Microstructural evolution and mechanical properties of maraging steel produced by wire + arc additive manufacture process, Mater. Charact. 143 (2018) 152–162. https://doi.org/10.1016/j.matchar.2017.12.002.

[13] J. Ge, J. Lin, Y. Chen, Y. Lei, H. Fu, Characterization of wire arc additive manufacturing 2Cr13 part: Process stability, microstructural evolution, and tensile properties, J. Alloys Compd. 748 (2018) 911–921. https://doi.org/10.1016/j.jallcom.2018.03.222.

[14] J. V. Gordon, C. V. Haden, H.F. Nied, R.P. Vinci, D.G. Harlow, Fatigue crack growth anisotropy, texture and residual stress in austenitic steel made by wire and arc additive manufacturing, Mater. Sci. Eng. A. 724 (2018) 431–438. https://doi.org/10.1016/j.msea.2018.03.075.

[15] W. Wu, J. Xue, L. Wang, Z. Zhang, Y. Hu, C. Dong, Forming process, microstructure, and mechanical properties of thin-walled 316L stainless steel using speed-cold-welding additive manufacturing, Metals (Basel). 9 (2019). https://doi.org/10.3390/met9010109.

[16] N. Rodriguez, L. Vázquez, I. Huarte, E. Arruti, I. Tabernero, P. Alvarez, Wire and arc additive manufacturing: a comparison between CMT and TopTIG processes applied to stainless steel, Weld. World. 62 (2018) 1083–1096. https://doi.org/10.1007/s40194-018-0606-6.

[17] L. Ji, J. Lu, C. Liu, C. Jing, H. Fan, S. Ma, Microstructure and mechanical properties of 304L steel fabricated by arc additive manufacturing, MATEC Web Conf. 128 (2017). https://doi.org/10.1051/matecconf/201712803006.

[18] C. V. Haden, G. Zeng, F.M. Carter, C. Ruhl, B.A. Krick, D.G. Harlow, Wire and arc additive manufactured steel: Tensile and wear properties, Addit. Manuf. 16 (2017) 115–123. https://doi.org/10.1016/j.addma.2017.05.010.

[19] L. Gardner, P. Kyvelou, C. Buchanan, Testing of Wire and Arc Additively Manufactured tubular sections, (2019) 978–981. https://doi.org/10.3850/978-981-11-0745-0.

[20] F. Hejripour, F. Binesh, M. Hebel, D.K. Aidun, Thermal modeling and characterization of wire arc additive manufactured duplex stainless steel, J. Mater. Process. Technol. 272 (2019) 58–71. https://doi.org/10.1016/j.jmatprotec.2019.05.003.

[21] V. Laghi, M. Palermo, G. Gasparini, V.A. Girelli, T. Trombetti, Experimental results for structural design of Wire-and-Arc Additive Manufactured stainless steel members, 2019.

[22] MX3D Webpage, (n.d.). www.mx3d.com.

[23] Oerlikon, (n.d.). https://www.oerlikon.com/en/.

[24] DIN EN 10002-1:2001, Metallic materials - Tensile testing, Met. Mater. - Tensile Test. (2001) 54.

[25] V. Laghi, M. Palermo, G. Gasparini, V.A. Girelli, T. Trombetti, Geometrical characterization of Wire-and-Arc Additive Manufactured steel elements, VBRI Press Adv. Mater. Lett. (2019).

[26] ASTM International, E3 Preparation of Metallographic Specimens, Annu. B. ASTM Stand. 11 (2017) 1–17. https://doi.org/10.1520/E0003-11R17.1.

[27] G.F. Vander Voort, G.M. Lucas, E.P. Manilova, Metallography and microstructures of stainless steels and maraging steels, Mater. Park. OH ASM Int. (2004) 670–700.

[28] R. Bourne, R. Bourne, ImageJ, Fundam. Digit. Imaging Med. 9 (2010) 185–188. https://doi.org/10.1007/978-1-84882-087-6_9.
[29] ASTM A276-16, Standard Specification for Stainless Steel Bars and Shapes, ASTM Int. (2016) 1–8. https://doi.org/10.1520/A0276.
[30] X. Xu, G. Mi, Y. Luo, P. Jiang, X. Shao, C. Wang, Morphologies, microstructures, and mechanical properties of samples produced using laser metal deposition with 316 L stainless steel wire, Opt. Lasers Eng. 94 (2017) 1–11. https://doi.org/10.1016/j.optlaseng.2017.02.008.
[31] W.J. Sames, F.A. List, S. Pannala, R.R. Dehoff, S.S. Babu, The metallurgy and processing science of metal additive manufacturing, Int. Mater. Rev. 61 (2016) 315–360. https://doi.org/10.1080/09506608.2015.1116649.
[32] S. Kou, Post-solidification phase transformations, in: Weld. Metall., 2003. https://doi.org/10.1002/0471434027.ch9.
[33] L. Hitzler, J. Hirsch, B. Heine, M. Merkel, W. Hall, A. Öchsner, On the anisotropic mechanical properties of selective laser-melted stainless steel, Materials (Basel). 10 (2017). https://doi.org/10.3390/ma10101136.
[34] G.E. Dieter, D.J. Bacon, Mechanical metallurgy, McGraw-hill, 1986.
[35] E.W. Hovig, A.S. Azar, F. Grytten, K. Sørby, E. Andreassen, Determination of anisotropic mechanical properties for materials processed by laser powder bed fusion, Adv. Mater. Sci. Eng. 2018 (2018). https://doi.org/10.1155/2018/7650303.
[36] T.H. Courtney, Mechanical behavior of materials, Waveland Press, 2005.
[37] EN 1993 1-4: Eurocode 3: Design of steel structures, part 1-4: General rules, supplementary rules for stainless steel, (2015).
[38] AS/NZS 4673: Cold-formed stainless steel structures, (2001).
[39] SEI/ASCE 08-02: Specification for the design of cold-formed stainless steel structural members, (1991).
[40] M.L. Griffith, M.T. Ensz, J.D. Puskar, C. V. Robino, J.A. Brooks, J.A. Phillibert, J.E. Smugeresky, W.H. Hofmeister, Understanding the microstructure and properties of components fabricated by laser engineered net shaping (LENS), MRS Online Proc. Libr. Arch. 625 (2000). https://doi.org/10.1111/jfb.12029.